ChemPubSoc Europe

DOI: 10.1002/chem.201406019

CHEMISTRY A European Journal Full Paper

Redox Chemistry |Hot Paper|

How a Redox-Innocent Metal Promotes the Formal Reductive Elimination of Biphenyl Using Redox-Active Ligands

Daniel Charles Ashley[a] and Mu-Hyun Baik*[a, b]

Abstract: One of the most compelling strategies for utilizing redox-active ligands is to perform redox events at the ligands to avoid accessing prohibitively high energy oxidation states at the metal center. This has been demonstrated experimentally in many systems, yet there is little understanding of the fundamental electronic structures involved with these transformations or how to control them. Here, the reductive elimination of biphenyl from $[M(isq)_2Ph_2]$ (M = Ti, Zr, and Hf and isq = 2,4-di-*tert*-butyl-6-*tert*-butyliminosemiquinone) was studied computationally. It was found that the metal remains in the +IV oxidation state and all redox chemistry was mediated by the redox-active ligands. Two types of electron-transfer mechanisms were identified, an asymmetric unpaired electron transfer (UET) and a symmetric pairwise electron transfer (PET), the former always being lower in energy. The energetic differences between these two mechanisms were explained through simple molecular orbital theory arguments. Despite the metal's redox-inactivity, it still has a marked influence on the calculated energetics of the reaction, with the Ti systems being much more reactive than the Zr/Hf systems. This primarily originates from the shorter Ti–Ph bond, which leads to a stronger filled-filled interaction between these ligands at the reactant state. This greater reactant destabilization leads to the lower activation energies.

Introduction

Oxidative additions are important for many catalytic processes in which small molecules are reductively activated, while the metal center is formally oxidized to form M–X bonds.[1] For example, carbon dioxide can react with a metal that has accessible valence electrons to form a metallacarboxylate, as shown in Scheme 1 a. Pioneering work by Wieghardt[2] and others[3] challenged this paradigm, recognizing that ligands that were classically thought to be innocent observers may supply the electrons needed for forming the M–X bond. This new paradigm allowed for adopting entirely new strategies for redox reaction design,[4] in which the formal oxidation state of the metal remains unchanged, as illustrated in Scheme 1 b. These redox-active ligands are not involved directly in the bond formation process, but serve as an electron reservoir and may allow for avoiding high oxidations states at the metal that give rise to high-energy intermediates. The scope of the redox reactions may be expanded by providing excess redox equivalents in addition to what the metal center can accommodate.[5]

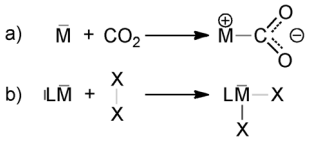

Scheme 1. a) Addition of CO_2 where the reducing equivalents come entirely from the metal. b) Oxidative addition where the electrons come entirely from the redox-active ligands.

Although this general principle is well appreciated, details of how these redox reactions occur are not well understood. One interesting example was presented by Heyduk,[6] in which dihalogens were added to d^0 group IV metal centers, carrying out what may be seen as an oxidative addition at a metal center in its highest oxidation state. Scheme 2 shows the complex $[Zr^{IV}(ap)_2(thf)_2]$ (**1**, ap^{2-} = 2,4-di-*tert*-butyl-6-*tert*-butylamidophenolate, see Figure 1) reacting with X_2 to form $[Zr^{IV}(isq)_2(X)_2]$ (**2**, isq^- = 2,4-di-*tert*-butyl-6-*tert*-butyliminosemiquinone). The same ligand was also used for the reverse reaction with $[Zr^{IV}(isq)_2Ph_2]$ (**4**), in which the redox-active ligands act as electron acceptors in the reductive elimination of biphenyl and form **1**, as summarized in Scheme 2.[7] These reactions are compelling examples of how redox-active ligands may be utilized to perform traditionally metal-based reactions. While several mechanistic studies were reported on related Co^{III} systems,[4b,8] no detailed analysis of the electronic rearrangements were performed. Recently, we investigated a catalytic Zr^{IV} system that also employs redox-active ligands, and we found that the metal remained "redox innocent" throughout catalysis.[9] How-

[a] D. C. Ashley, M.-H. Baik
Department of Chemistry, Indiana University
800 East Kirkwood Avenue
Bloomington, Indiana 47405 (USA)
E-mail: mbaik@indiana.edu

[b] M.-H. Baik
Department of Materials Chemistry
Korea University, Sejong 339–700 (South Korea)

Supporting information for this article is available on the WWW under http://dx.doi.org/10.1002/chem.201406019.

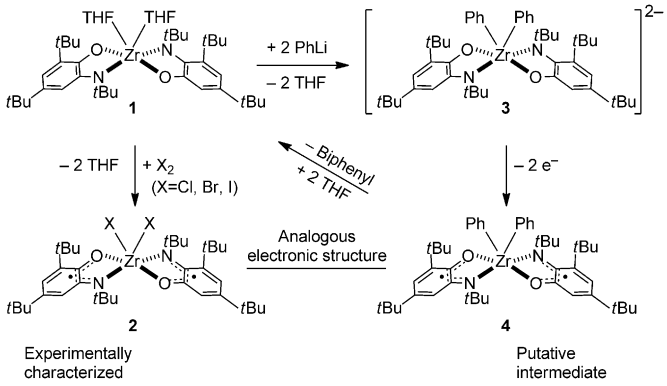

Scheme 2. Summary of experimental work performed with the $Zr^{IV}(isq)_2$ system.

ever, in general, the role that the metal plays in these reactions remains poorly understood.

Is the metal simply a scaffolding Lewis acid that holds the redox-active ligands in place? Or does it play a more decisive role in controlling the transformation? To answer these questions density functional methods were applied to explore the role of the redox-active ligands and the metal in the reductive elimination of biphenyl by the $[Zr^{IV}(isq)_2Ph_2]$. If the chemistry is entirely mediated by the redox-active ligands we expect the frontier MOs to be ligand-based, thus making the metal "redox innocent" throughout the reaction. To further explore this concept, the putative Ti and Hf analogues were also studied. The results of this work suggest that even though the redox chemistry is dominated by the ligands, the metal can still play a critical role in tuning the reactivity.

Results and Discussion

The most intriguing question is: how intimately involved is the metal in the electron transfer? As shown in Scheme 2, phenylation of **1** produced the dianionic complex **3**, which upon oxidation formed the reactant **4. 4** was only fleetingly characterized by UV/Vis spectroscopy, is believed to be an analogue of the well-characterized species $[M(isq)_2X_2]$ (see Scheme 2), which adopts a ligand-centered diradical open-shell singlet state[6b] based on the large distance between the two iminosemiquinone ligands and the EPR data. Indeed, the antiferromagnetically (AF) coupled singlet with each isq^- ligand carrying one electron with opposite spin was found to be lower in energy than the closed-shell (CS) singlet analogue. Similarly, the AF-coupled singlet is the ground state for the Ti and Hf analogues (see Table 1); consistent with weak coupling, the triplet is almost isoenergetic with the AF singlet. This finding is different from a similar Zr^{IV} complex, for which the CS singlet was lower in energy,[10] due to geometrical differences. In the previous work the redox-active ligands were able to overlap their singly occupied molecular orbitals (SOMOs) by forming a π–π interaction. The geometry of the $[M(isq)_2Ph_2]$ systems studied here does not allow this type of strong interaction between the ligands, and hence only weak AF coupling is observed.

Table 1. Spin-state energetics for $[M(isq)_2Ph_2]$ complexes. Note that the trends in ΔG_{sol} are dominated by the trends in electronic energy. All values listed are in kcal mol^{-1}.

Spin state	Ti ΔG_{sol} (ΔE)	Zr ΔG_{sol} (ΔE)	Hf ΔG_{sol} (ΔE)
AF singlet	0.00	0.00	0.00
triplet	1.17 (2.77)	0.17 (1.61)	0.12 (1.36)
CS singlet	2.97 (3.09)	5.14 (5.07)	5.70 (5.56)

The computed extent of AF coupling is dependent on the density functional applied. Here, we employ B3LYP,[11] but when a non-hybrid functional is used,[10] the spin densities on the isq ligands decrease (see Supporting Information) and the closed-shell configuration becomes more prevalent—this is a serious, and widely recognized problem in broken-symmetry (BS) DFT.[12] In lieu of experimental data, higher level multireference methods, such as CASSCF, should be employed.[13] The $[Zr(isq)_2Ph_2]$ complex is far too fleeting to experimentally verify our calculations, but we can calibrate our methodology with $[Zr(isq)_2Cl_2]$ (vide supra). The B3LYP results for $[Zr(isq)_2Cl_2]$ agree with the weak-coupling picture expected from experiment, and they are similar to our calculated results for $[Zr(isq)_2Ph_2]$ in terms of spin and energetics. As the B3LYP results match a similar experimentally studied system and the same results for $[Zr(isq)_2Ph_2]$ are obtained it appears plausible for our system; however, it is important to be cautious. Benchmarking studies against high-level CASSCF calculations are currently ongoing in our laboratory.

The relevant frontier MOs of the AF-coupled and CS singlet states are shown in Figure 2. As expected, the CS singlet

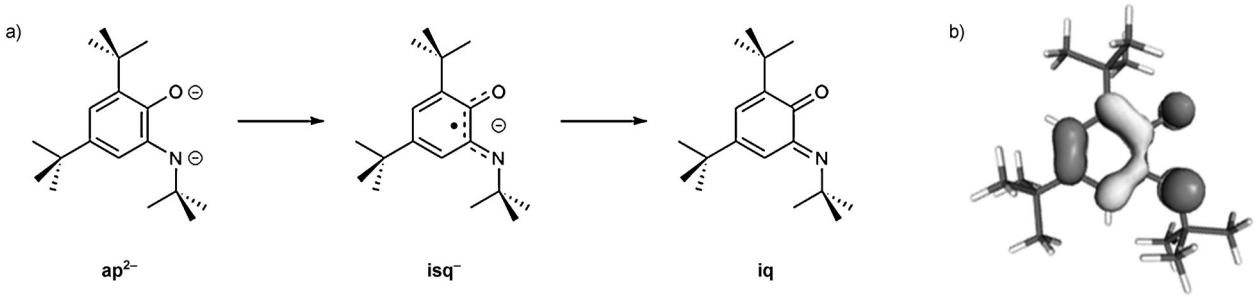

Figure 1. a) Three possible oxidation states of the redox-active ligand. b) Redox-active molecular orbital (isovalue: 0.05 au).

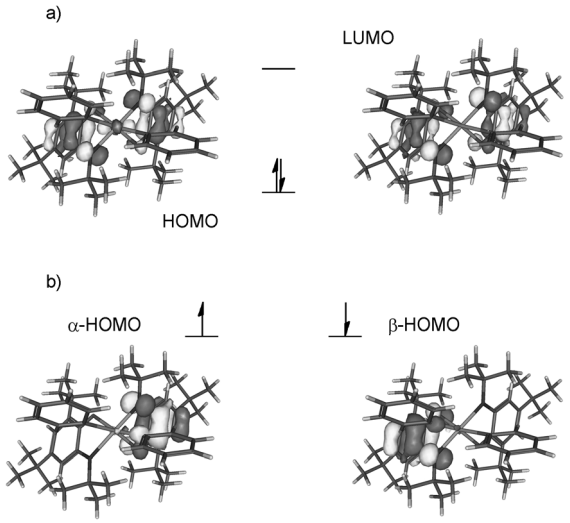

Figure 2. Isosurface plots (iso values: 0.05 au) of relevant MOs. a) HOMO and LUMO of closed-shell singlet $[Zr(isq)_2Ph_2]$. b) SOMOs of AF-coupled singlet $[Zr(isq)_2Ph_2]$.

shows purely ligand–π*-based MOs: they are the in-phase (HOMO) and out-of-phase (LUMO) combinations of the isq^- fragment orbital shown in Figure 1. In the AF-coupled analogue, these two MOs decouple from each other and become localized, BS orbitals of the ligand–π* type. Analysis of the Mulliken spin density indicates weak coupling with one unpaired electron placed on each isq^- ligand (Table 2). Note the lack of any spin on the metal, supporting the assignment of M^{IV}.

Table 2. Mulliken spin densities for reactants/transition states.

Fragment	Ti R/TS	Zr R/TS	Hf R/TS
M	0.00/−0.05	0.00/−0.04	0.00/−0.07
L1[a]	0.79/0.94	0.86/0.93	0.88/0.87
L2[a]	−0.79/−0.74	−0.87/−0.33	−0.88/−0.13
Ph1[b]	−0.02/−0.14	−0.02/−0.32	−0.02/−0.38
Ph2[b]	0.02/−0.01	0.02/−0.22	0.02/−0.30

[a] Sum of spins on each isq^-/ap^{2-} ligand. [b] Sum of spins on the phenyl rings.

While the AF-coupled state has the lowest energy, it may not be associated with the lower energy barrier for reductive elimination. Thus, transition states were located for both the AF and CS configurations, and we found two distinct mechanisms of electron transfer, as described in Scheme 3. The transition state located for the AF state showed a significant increase in β-spin density on the phenyl moieties accompanied by a matching reduction of β-spin on one of the two isq^- radical ligands, which can formally be considered an ap^{2-} ligand (Table 2). In addition, there is also a modest increase in the α-spin of the remaining isq^- ligand. This mechanism, in which only one redox-active ligand was reduced at the transition state, was also evidenced by dramatically different bond lengths between the metal and the redox-active ligands, with

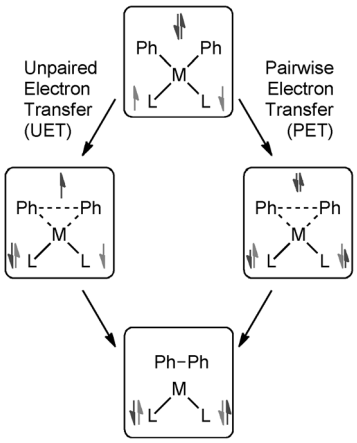

Scheme 3. Mechanisms of electron transfer studied.

Table 3. Select bond lengths [Å] from AF coupled reactants/transition states for $[M(isq)_2Ph_2]$. N1/O1 refers to the coordinating nitrogen and oxygen atoms for L1 as identified in Table 2.

	Ti R/TS	Zr R/TS	Hf R/TS
M–N1	2.19/2.50	2.32/2.58	2.30/2.49
M–O1	1.98/1.91	2.16/2.08	2.12/2.05
M–N2	2.19/2.21	2.32/2.26	2.30/2.22
M–O2	1.98/1.91	2.16/2.04	2.12/2.00

the reduced ligand naturally showing much shorter bonds (Table 3). The structural changes are often far more dramatic than the spin density changes and are more useful as diagnostic indicators of the oxidation state of the ligand for these transition states, especially in the Ti case. Given that the electron transfer involves one electron at the transition state, we refer to this mechanism as unpaired electron transfer (UET). The closed-shell transition state cannot transfer one electron to one-individual ligand, because its LUMO is delocalized over both redox-active ligands. Hence, a pair of electrons will be partially transferred to both redox-active ligands simultaneously at the transition state, thus giving rise to a pairwise electron transfer (PET) mechanism.

Interestingly, the UET mechanism was substantially more accessible than the PET mechanism for each metal (Table 4). In the case of $[Ti(isq)_2Ph_2]$, the barrier for UET was only 5.95 kcal mol^{-1}, compared to the PET process that was 18.00 kcal mol^{-1}. In addition, the Ti complex had notably lower barriers than

Table 4. Energetics for reductive elimination [kcal mol^{-1}]. All numbers are relative to the AF singlet reactants.

M^{IV}	PET $\Delta G^{\ddagger}_{sol}$ ($\Delta E^{\ddagger}$)	UET $\Delta G^{\ddagger}_{sol}$ ($\Delta E^{\ddagger}$)
Ti	18.00 (17.32)	5.95 (9.13)
Zr	23.01 (22.69)	12.53 (16.51)
Hf	24.44 (23.54)	17.58 (19.28)

either the Zr or Hf complexes, which were similar to each other and particularly so, when only the electronic energies are considered. There is a small additional entropic penalty at the transition state for the UET mechanism in the Hf complex due to noise in the low-lying vibrational modes, rendering this small free-energy difference physically meaningless. The UET transition states also benefit from modest gains in the solvation energy (solvent = THF) compared to the PET due to the asymmetric charge transfer, which gives rise to an increase of the molecular dipole moment, as the transition state is reached.

The isq ligands have bulky *tert*-butyl groups that enforce a pseudo-octahedral geometry constraining the phenyl rings to be almost co-planar with each other. Unfortunately, the reactant complexes were not isolated and characterized, so we cannot compare our calculated structures to experiments. However, our structures are in good agreement with the experimentally confirmed structures of the $[M(isq)_2X_2]$ species.[6b] These pseudo-octahedral structures are incapable of directly forming biphenyl and the complex must dramatically distort at the transition state by forming a square-pyramidal-like structure to orient the phenyl groups towards making biphenyl. This structural distortion is shown in Figure 3 for Ti, in which

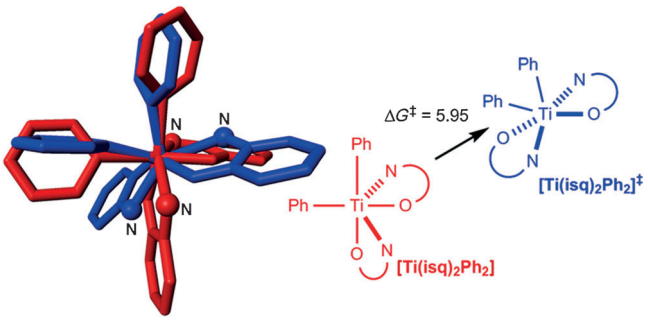

Figure 3. Structural changes observed, as the transition state is reached.

the redox-active ligands moved away from each other, and significantly rotated about the phenyl rings.

Why is asymmetrically transferring an electron to one specific redox-active ligand more favorable than transferring a pair of electrons to one delocalized orbital? To address this question it is necessary to examine the MOs that serve as the electron acceptors. Figure 4a illustrates the formation of the CS

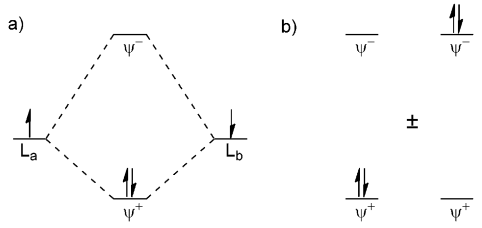

Figure 4. a) Single-configurational MO diagram for pairing up electrons on redox-active ligands. b) Dominant configurations involved in the description of an AF-coupled singlet.

singlet case. Any transfer of electrons from the biphenyl moiety will have to be directed into the LUMO of this species. This LUMO will be significantly higher in energy than the energies of the non-interacting redox-active orbitals. By being forced to transfer a pair of electrons into the LUMO, the restricted solution will naturally be predisposed towards a higher energy barrier. However, this does not mean that simply treating the system as a BS singlet will naturally lead to lower barriers either. It is important to recall that the BS approximation simulates the density of the multiconfigurational picture shown in Figure 4b. Here, the true diradical singlet can be expressed as a linear combination of two configurations, $\psi^+(1)(2)$ and $\psi^-(1)(2)$.[14]

While it is difficult to visualize transferring electrons into a multiconfigurational wavefunction, one evident conclusion is that as electrons are transferred into this symmetric system the excitations into the ψ^- will have to increase, and hence we are still increasing the population of this higher energy orbital. If this interpretation is correct, a BS-singlet transition state that shows symmetrical transfer of electrons into the redox-active ligands (BS-PET) should have a higher energy than the UET transition states shown already assuming it is accurately modeling the true multiconfigurational system. Unfortunately, it was exceedingly difficult to locate both the UET transition state and a BS-PET state for the same molecule. In fact, no BS-PET transition states could be located at all for the $[M(isq)_2Ph_2]$ species, but they could be located in some instances for a small model system in which the *tert*-butyl groups of isq^- were replaced by methyl groups, denoted as isq^{Me}.

Activation energies and spin densities are shown for the $[M(isq^{Me})_2Ph_2]$ species in Tables 5 and 6, respectively. In the case of $[Ti(isq^{Me})Ph_2]$ only the BS-PET transition state could be found. Recall that the UET transition state for $[Ti(isq)_2Ph_2]$ was about 10 kcal mol^{-1} lower in energy than the PET transition

Table 5. Energetics for reductive elimination [kcal mol^{-1}] of $[M(isq^{Me})_2Ph_2]$ species. All numbers are relative to the AF singlet reactants.

M^{IV}	CS-PET $\Delta G^{\ddagger}_{sol}$ ($\Delta E^{\ddagger}$)	BS-PET $\Delta G^{\ddagger}_{sol}$ ($\Delta E^{\ddagger}$)	UET $\Delta G^{\ddagger}_{sol}$ ($\Delta E^{\ddagger}$)
Ti	10.79 (7.70)	9.53 (7.13)	N/A
Zr	21.85 (18.79)	N/A	16.97 (16.00)
Hf	18.53 (17.04)	18.80 (16.72)	13.47 (13.95)

Table 6. Mulliken spin densities for reactants/transition states of $[M(isq^{Me})_2Ph_2]$ species.

Fragment	Ti (BS-PET) R/TS	Zr (UET) R/TS	Hf (UET) R/TS	Hf (BS-PET) R/TS
M	0.00/0.01	0.00/0.04	0.00/0.02	0.00/0.00
L1[a]	−0.86/−0.52	−0.92/−0.81	−0.92/−0.76	−0.92/−0.38
L2[a]	0.86/0.47	0.92/0.12	0.92/0.09	0.92/0.39
Ph1[b]	0.02/0.09	−0.01/0.36	−0.01/0.34	−0.01/−0.05
Ph2[b]	−0.02/−0.04	0.01/0.28	0.01/0.30	0.01/0.05

[a] Sum of spins on each isq^-/ap^{2-} ligand. [b] Sum of spins on the phenyl rings.

state. All the [M(isq^{Me})Ph$_2$] barriers are already significantly lower in energy than their full model counterparts, with the CS-PET electronic barrier for [Ti(isq^{Me})Ph$_2$] being only 7.70 kcal mol^{-1}. Assuming that the UET transition state is also about 10 kcal mol^{-1} lower for the small model system, then it would be essentially barrierless and impossible to locate. It is not clear, however, why the transition state on the BS potential energy surface for the PET process involving [Zr(isq^{Me})$_2$Ph$_2$] cannot be located. What is most important is that in each case where the BS-PET transition state could be located it was effectively isoenergetic with the CS-PET transition state. This finding demonstrates that the energy difference between UET and PET is not just a function of the computational method, that is, unrestricted vs. restricted singlets, but rather arises from the avoidance of transferring electrons into the LUMO shown in Figure 4a. The only way that UET can occur is if the molecule distorts its structure to a lower symmetry, in this case from C_2 to C_1, thereby removing the degeneracy of the isq$^-$ ligands, making one a better electron acceptor than the other. For either the PET or UET case the actual mechanism of electron transfer from the ligands is relatively simple and illustrated in Scheme 4. As the two phenyl groups move closer together

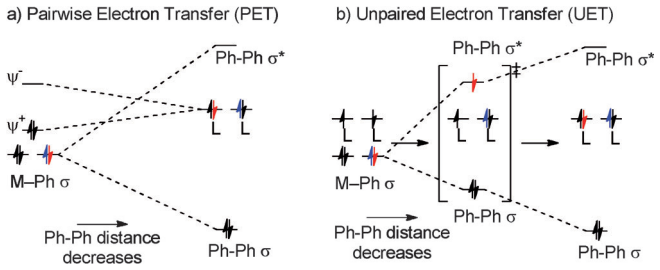

Scheme 4. Electronic structure rearrangements for mechanisms of electron transfer studied.

they create a significant filled–filled interaction involving the M–Ph σ bonds. These orbitals gradually transform into the Ph–Ph σ and Ph–Ph σ* orbitals as the C–C distance decreases. Eventually the filled Ph–Ph σ* orbital becomes high enough in energy to transfer its electrons into the isq$^-$ ligand orbitals through either the PET or UET mechanism. At the completion of the reaction a pair of electrons will have been transferred to the metal complex from the [Ph$_2$]$^{2-}$ group and a C–C bond will have been formed thereby making free biphenyl.

The MOs and Mulliken spin densities described above show that the metal is not involved in the electron-transfer, yet the Ti complex is predicted to be much more reactive than its Zr and Hf counterparts. What is the metal's role in this mechanism? Table 7 compares the overall reaction energies for forming the [M(ap)$_2$] complexes and liberating biphenyl. The [Zr(ap)$_2$(thf)$_2$] complex was previously detected experimentally[7] as the final product of this reaction, but the calculated energies show that binding THF is unfavorable and the [M(ap)$_2$] species are more stable in solution. Regardless of the nature of the final product, the putative [M(ap)$_2$] species will be the immediate resulting product of the reductive elimination step.

Table 7. Thermodynamic driving force and key energetic components to metal-influenced reactivity. All reaction energetics are in kcal mol^{-1}.

M^{IV}	Product formation ΔG_{sol} (ΔE)	ΔE_{prep} (Ph–Ph)
Ti	−106.97 (−88.07)	50.96
Zr	−81.31 (−65.72)	43.05
Hf	−79.82 (−63.58)	43.17

The trends in the overall reaction energies are similar to what is observed for the barrier heights and suggests a Hammond-type of reaction scenario, that is, the lowering of the transition state energy results from a higher energy reactant state that makes Ti more reactive, when compared to its congeners. This destabilization could either result from increased unfavorable interactions between the two phenyl groups, or less favorable interactions between the phenyl groups and Ti.

While the second and third row metal complexes should have stronger bonds than their first row analogues, making the Ti–Ph bonds the easiest to break, another explanation is offered by the optimized [M(isq)$_2$Ph$_2$] structures. The C–C distance of the *ipso*-phenyl carbon atoms is 3.13 Å for [Ti(isq)$_2$Ph$_2$], but much longer at 3.42 Å for [Zr(isq)$_2$Ph$_2$] and [Hf(isq)$_2$Ph$_2$]. As Zr and Hf are much larger than Ti and of similar size to each other, due to the lanthanide contraction, they naturally have longer M–L bonds. At the UET and PET transition states these C–C distances are nearly identical for all three metals at about 2.24 Å and 2.33 Å, respectively; thus, the two phenyl groups are drawn closer, and therefore experience more Coulombic repulsion. As shown in Scheme 4, an intrinsic part of the reductive elimination barrier is the filled–filled interaction between the two phenyl groups that are forming a bond and transferring electrons back to the metal complex. For [Ti(isq)$_2$Ph$_2$] part of the energy needed to reach the transition state has already been paid for at the reactant stage by forcing the Ph groups to be much closer than in the Zr and Hf cases, and hence it takes less energy to reach the transition state. The Coulombic repulsion experienced by the bound phenyl anions can be quantified by calculating the electronic energies of the phenyls at their geometries in the optimized complex and comparing that to the energy of the separated free ligands. The energy penalty of bringing the free ligands together into the geometry found in the molecular entity is often referred to as the preparation energy (ΔE_{prep}) when discussed in terms of energy decomposition analysis.[15] ΔE_{prep} is tabulated in Table 7 for the Ph ligands of the AF-coupled [M(isq)$_2$Ph$_2$] complexes. As expected ΔE_{prep} is about 8 kcal mol^{-1} more positive for Ti than Zr and Hf. Given that the increase in ΔE_{prep} for Ti is almost identical to the lowering of $\Delta E^{\ddagger}$ for Ti, we propose that this reactant destabilization is the primary reason for its increased reactivity towards elimination of the biphenyl.

Conclusion

As the inorganic community's enthusiasm for utilizing redox-active ligands in catalytic and stoichiometric reactions grows,

our understanding of the physical and chemical concepts necessary to control and modulate reactions must grow as well. The reductive elimination of biphenyl by $[M(isq)_2Ph_2]$, while not necessarily one of great interest for catalytic design due to its simplicity and the irreversible nature of the reaction, is an instructive model for both experimentalists and theorists to study how the identity of the metal can tune the energetics of redox-active ligand mediated reactions. By thoroughly analyzing the electronic structure re-arrangements and different mechanisms of electron transfer it was clear that the metal was completely redox-innocent throughout the reaction, and that the electron transfer events were entirely ligand based. This made it possible to ascertain the role the AF coupling of the ligands played in promoting the reaction, and understand why in a situation where weak AF coupling was involved it would be energetically preferable to asymmetrically transfer electrons from the substrate to the redox-active ligands. Because the metal was not electronically involved in the redox reaction, its secondary effects on the reaction energetics, which were quite significant, were also readily decomposed. That changing the metal from 2nd or 3rd row to 1st row could reduce the barrier by about 10 kcal mol^{-1} was surprising and exciting given that the metal itself was uninvolved. By analyzing the overall thermodynamics of the reaction and the structure of the reactants it was determined that the metal could influence the reactivity by destabilizing the reactant by already paying part of the initial cost of the Ph–Ph repulsion at the reactant stage. This destabilization was induced by the structural constraints of the smaller Ti atom and appeared to completely explain the observed trend in the calculated kinetics of biphenyl elimination.

Computational Methods

Calculations were carried out using DFT as implemented in the Jaguar 7.7 suite of ab initio quantum chemistry programs.[16] Geometry optimizations were performed with the B3LYP functional using the 6-31G** basis set.[17] Transition metals were represented using the Los Alamos LACVP basis that includes relativistic effective core potentials.[18] The energies of the optimized structures were reevaluated by additional single point calculations on each optimized geometry using Dunning's correlation consistent triple-ζ basis set cc-pVTZ(-f) that includes a double set of polarization functions.[19] For transition metals, we used a modified version of LACVP, designated as LACV3P, in which the exponents were decontracted to match the effective core potential with triple-ζ quality. Vibrational/rotational/translational entropies of the solute(s) were included using standard thermodynamic approximations. Solvation energies were evaluated by a self-consistent reaction field (SCRF) approach based on accurate numerical solutions of the linearized Poisson–Boltzmann equation.[20] Solvation calculations were carried out at the optimized gas phase geometry employing the dielectric constant of $\varepsilon = 7.6$ (THF). As is the case for all continuum models, the solvation energies are subject to empirical parameterization of the atomic radii that are used to generate the solute surface. We employed the standard set of optimized radii for H (1.150 Å), C (1.900 Å), N (1.600 Å), O (1.600 Å), Ti (1.587 Å), Zr (1.562 Å), and Hf (1.571 Å). Convergence to plausible electronic states that correspond to conceptually meaningful electronic configurations was monitored by carefully observing the Mulliken spin densities and visualizing the frontier molecular orbitals. When multiple minima were encountered, we compared the total energies and chose the structure with the lowest energy. AF singlet states were modeled using Noodleman's broken symmetry (BS) formalism without spin projection.[21] Energy components were computed as follows following the protocol of our previous work. The change in solution phase free energy ΔG_{sol} was calculated by using Equations (1)–(3), in which ΔG_{gas} = change in gas phase free energy; $\Delta\Delta G_{solv}$ = change in free energy of solvation; ΔH_{gas} = change in gas phase enthalpy; T = temperature (298.15 K); ΔS_{gas} = change in gas phase entropy; ΔE_{SCF} = self consistent field energy, that is, "raw" electronic energy as calculated at the triple-ζ level; ΔZPE = change in vibrational zero point energy. All structures were determined to be minima with no imaginary frequencies, or in the case of transition states, exactly one imaginary frequency.

$$\Delta G_{sol} = \Delta G_{gas} + \Delta\Delta G_{solv} \quad (1)$$

$$\Delta G_{gas} = \Delta H_{gas} - T\Delta S_{gas} \quad (2)$$

$$\Delta H_{gas} = \Delta E_{SCF} + \Delta ZPE \quad (3)$$

Acknowledgements

We thank the NSF(0116050, CHE-0645381, CHE-1001589) and the Research Corporation (Scialog Award to M.H.B.) for support. This work was supported by the Center for Sustainable Use of Renewable Feedstocks (CenSURF), an NSF Center for Chemical Innovation (CHE-1240194).

Keywords: electron transfer · Group IV metals · reaction mechanisms · redox-active ligands · reductive elimination

[1] R. H. Crabtree, *The Organometallic Chemistry of the Transition Metals*, Wiley Interscience, New York (USA), **2001**.
[2] P. Chaudhuri, C. N. Verani, E. Bill, E. Bothe, T. Weyhermüller, K. Wieghardt, *J. Am. Chem. Soc.* **2001**, *123*, 2213–2223.
[3] R. Eisenberg, H. B. Gray, *Inorg. Chem.* **2011**, *50*, 9741–9751.
[4] a) W. Kaim, *Inorg. Chem.* **2011**, *50*, 9752–9765; b) W. I. Dzik, J. I. van der Vlugt, J. N. H. Reek, B. de Bruin, *Angew. Chem. Int. Ed.* **2011**, *50*, 3356–3358; *Angew. Chem.* **2011**, *123*, 3416–3418; c) M. R. Ringenberg, S. L. Kokatam, Z. M. Heiden, T. B. Rauchfuss, *J. Am. Chem. Soc.* **2008**, *130*, 788–789; d) I. M. Lorkovic, R. R. Duff, M. S. Wrighton, *J. Am. Chem. Soc.* **1995**, *117*, 3617–3618; e) J. L. Boyer, J. Rochford, M.-K. Tsai, J. T. Muckerman, E. Fujita, *Coord. Chem. Rev.* **2010**, *254*, 309–330; f) P. J. Chirik, K. Wieghardt, *Science* **2010**, *327*, 794–795; g) C. A. Lippert, S. A. Arnstein, C. D. Sherrill, J. D. Soper, *J. Am. Chem. Soc.* **2010**, *132*, 3879–3892; h) S. Ghosh, M. H. Baik, *Inorg. Chem.* **2011**, *50*, 5946–5957; i) K. Wang, E. I. Stiefel, *Science* **2001**, *291*, 106–109; j) K. Ray, T. Petrenko, K. Wieghardt, F. Neese, *Dalton Trans.* **2007**, 1552–1566; k) Y. Dede, X. H. Zhang, M. Schlangen, H. Schwarz, M. H. Baik, *J. Am. Chem. Soc.* **2009**, *131*, 12634–12642; l) J. T. Muckerman, D. E. Polyansky, T. Wada, K. Tanaka, E. Fujita, *Inorg. Chem.* **2008**, *47*, 1787–1802.
[5] V. Lyaskovskyy, B. de Bruin, *ACS Catal.* **2012**, *2*, 270–279.
[6] a) K. J. Blackmore, J. W. Ziller, A. F. Heyduk, *Inorg. Chem.* **2005**, *44*, 5559–5561; b) K. J. Blackmore, M. B. Sly, M. R. Haneline, J. W. Ziller, A. F. Heyduk, *Inorg. Chem.* **2008**, *47*, 10522–10532.
[7] M. R. Haneline, A. F. Heyduk, *J. Am. Chem. Soc.* **2006**, *128*, 8410–8411.
[8] a) A. L. Smith, K. I. Hardcastle, J. D. Soper, *J. Am. Chem. Soc.* **2010**, *132*, 14358–14360; b) A. L. Smith, L. A. Clapp, K. I. Hardcastle, J. D. Soper, *Polyhedron* **2010**, *29*, 164–169.

[9] a) A. I. Nguyen, R. A. Zarkesh, D. C. Lacy, M. K. Thorson, A. F. Heyduk, *Chem. Sci.* **2011**, *2*, 166 – 169; b) S. Ghosh, M. H. Baik, *Chem. Eur. J.* **2015**, *21*, 1780 – 1789.
[10] N. A. Ketterer, H. J. Fan, K. J. Blackmore, X. F. Yang, J. W. Ziller, M. H. Baik, A. F. Heyduk, *J. Am. Chem. Soc.* **2008**, *130*, 4364 – 4374.
[11] a) A. D. Becke, *Phys. Rev. A* **1988**, *38*, 3098 – 3100; b) A. D. Becke, *J. Chem. Phys.* **1993**, *98*, 5648 – 5652; c) S. H. Vosko, L. Wilk, M. Nusair, *Can. J. Phys.* **1980**, *58*, 1200 – 1211; d) C. Lee, W. Yang, R. G. Parr, *Phys. Rev. B* **1988**, *37*, 785 – 789; e) P. J. Stephens, F. J. Devlin, C. F. Chabalowski, M. J. Frisch, *J. Phys. Chem.* **1994**, *98*, 11623 – 11627.
[12] a) W. M. C. Sameera, J. E. McGrady, *Dalton Trans.* **2008**, 6141 – 6149; b) C. Herrmann, M. Podewitz, M. Reiher, *Int. J. Quantum Chem.* **2009**, *109*, 2430 – 2446.
[13] K. Pierloot, H. Zhao, S. Vancoillie, *Inorg. Chem.* **2010**, *49*, 10316 – 10329.
[14] L. Salem, C. Rowland, *Angew. Chem. Int. Ed. Engl.* **1972**, *11*, 92 – 111; *Angew. Chem.* **1972**, *84*, 86 – 106.
[15] a) R. L. Lord, M.-H. Baik, *Inorg. Chem.* **2008**, *47*, 4413 – 4420; b) T. Ziegler, A. Rauk, *Theor. Chim. Acta* **1977**, *46*, 1 – 10; c) G. te Velde, F. M. Bickelhaupt, E. J. Baerends, C. F. Guerra, S. J. A. van Gisbergen, J. G. Snijders, T. Ziegler, *J. Comput. Chem.* **2001**, *22*, 931 – 967.
[16] Jaguar, version 7.7, Schrodinger, LLC, New York, NY, **2010**.
[17] V. Rassolov, J. A. Pople, M. Ratner, T. L. Windus, *J. Chem. Phys.* **1998**, *109*, 1223 – 1229.
[18] a) P. J. Hay, W. R. Wadt, *J. Chem. Phys.* **1985**, *82*, 270 – 283; b) W. R. Wadt, P. J. Hay, *J. Chem. Phys.* **1985**, *82*, 284 – 298.
[19] T. H. Dunning, Jr., *J. Chem. Phys.* **1989**, *90*, 1007 – 1023.
[20] a) B. Marten, K. Kim, C. Cortis, R. A. Friesner, R. B. Murphy, M. N. Ringnalda, D. Sitkoff, B. Honig, *J. Phys. Chem.* **1996**, *100*, 11775 – 11788; b) M. Friedrichs, R. Zhou, S. R. Edinger, R. A. Friesner, *J. Phys. Chem. B* **1999**, *103*, 3057 – 3061; c) S. R. Edinger, C. Cortis, P. S. Shenkin, R. A. Friesner, *J. Phys. Chem. B* **1997**, *101*, 1190 – 1197; d) A. A. Rashin, B. Honig, *J. Phys. Chem.* **1985**, *89*, 5588 – 5593.
[21] a) L. Noodleman, *J. Chem. Phys.* **1981**, *74*, 5737 – 5743; b) L. Noodleman, T. Lovell, W.-G. Han, J. Li, F. Himo, *Chem. Rev.* **2004**, *104*, 459 – 508; c) L. Noodleman, E. R. Davidson, *Chem. Phys.* **1986**, *109*, 131 – 143.

Received: November 7, 2014
Published online on February 4, 2015